JOURNAL OF AIRCRAFT
Vol. 39, No. 2, March–April 2002

Perturbation Analysis of Nonlinear Wheel Shimmy

James T. Gordon*
The Boeing Company, Seattle, Washington 98124

A perturbation analysis of nonlinear wheel shimmy in aircraft landing gear is presented for nonlinear models that include terms due to coulomb friction between the oleo struts and freeplay in the torque links. The method of multiple timescales is used to obtain general expressions for the limit-cycle amplitude and the frequency that are functions of ground speed. The analysis shows that stable or unstable limit cycles can exist for taxi speeds above or below a critical value with stability of the limit cycles being determined by the sign of a computed coefficient. When only coulomb friction is present, an unstable limit cycle exists. When only freeplay is present, a stable limit cycle exists. When both coulomb friction and freeplay are present, it is shown that stable and unstable limit cycles and a turning point can exist depending on the system parameter values. The solution method is applied to a simple shimmy model, and results from the perturbation analysis are shown to be in good agreement with those obtained by direct numerical integration of the nonlinear shimmy equations.

Nomenclature

A	=	response amplitude
$\hat{\boldsymbol{F}}_j, \hat{\boldsymbol{F}}_k$	=	vectors of nonlinear terms
$\boldsymbol{f}_{\text{cf}}$	=	vector of coulomb friction terms
$\boldsymbol{f}_{\text{fp}}$	=	vector of nonlinear stiffness terms including freeplay effects
$\boldsymbol{f}_j^{(n)}, \boldsymbol{f}_k^{(n)}$	=	Fourier coefficient vectors
i	=	imaginary unit, $\sqrt{-1}$
$\boldsymbol{K}, \bar{\boldsymbol{K}}$	=	stiffness matrices
$\boldsymbol{K}^{(0)}$	=	ϵ^0-order term in expansion for $\boldsymbol{K}$
$\boldsymbol{K}^{(1)}$	=	ϵ^1-order term in expansion for $\boldsymbol{K}$
$\boldsymbol{M}, \bar{\boldsymbol{M}}$	=	mass matrices
$\boldsymbol{q}$	=	vector of state variables
$\boldsymbol{q}_m$	=	coordinate vector in expansion for $\boldsymbol{q}$
V	=	system parameter (ground speed)
V_i	=	ith-order term in expansion for V
V_0	=	critical value of V
α	=	complex coefficient
β	=	complex coefficient
γ	=	complex coefficient
δ	=	complex coefficient
ϵ	=	small parameter
τ	=	independent variable time
τ_m	=	multiple timescales
ψ	=	phase
ω	=	frequency, dependent on amplitude A
ω_0	=	eigenvalue for V_0 and det $\boldsymbol{L}_0$

I. Introduction

THE prevention of landing gear shimmy continues to be an important area of concern in the design and operation of aircraft. Typically, both linear and nonlinear shimmy analyses are conducted, and by appropriate changes in the geometric, damping, and structural parameters, a shimmy-free configuration is sought. In general, linear models will fail to predict accurately the behavior of the inherently nonlinear landing gear system, although basic characteristics and trends usually will be determined correctly. The presence of coulomb friction between the oleo struts, freeplay in the torque links connecting the inner and outer struts, and hydraulic dampers or steering units challenges the analyst and further complicates modeling efforts. In addition, the tire–ground forces and moments are nonlinear functions of the tire slip angle.

Analytical solutions to nonlinear shimmy models have appeared in the published literature in only a few cases. Pacejka[1] presented a detailed study of the nonlinear shimmy of automobiles including a nonlinear tire theory and investigations of the effects of dry friction in the kingpins and wheel bearing clearance on shimmy. His results identified limit cycles using an analytical method by Magnus based on the harmonic balance method of Krylov and Bogoliubov[2] to linearize the equations. His results[1] also indicated that linear tire theories produce substantially the same results as the nonlinear except in regions of high slippage. Collins[3] has emphasized this latter point.

Gordon and Merchant[4] have applied the method of multiple-timescales to the analysis of nonlinear shimmy models for landing gear that include terms due to velocity squared damping. Burton[5] has applied the describing function method to the analysis of nonlinear shimmy models with a complete model of hydraulic steering cylinders used as dampers on a nose landing gear. Somieski[6] has used describing function methods for aircraft shimmy models with nonlinear representations of the tire aligning moment and side force.

The Krylov–Bogoliubov [(K–B) or harmonic balance][2] and describing function methods have been applied successfully to systems with relay-type nonlinearities having discontinuous jumps, for example, coulomb friction, freeplay, and hysteresis. Application of these procedures is justified, even with strong nonlinearities if the system possesses a filtering property that attenuates responses at the higher harmonic frequencies, that is, the system admits a periodic solution dominated by the fundamental harmonic. Popov[7] has given the conditions that must be satisfied by the system and the nonlinear function for the K–B averaging method to be applicable. In general, system models for nonlinear flutter and shimmy problems exhibit this filtering property. Shen[8] has discussed the suitability and application of the K–B method to nonlinear flutter problems. Šiljak[9] discussed the applicability criterion of Popov[7] in considerable detail for the describing function and K–B methods, including extensions to systems having multiple nonlinearities of symmetric and nonsymmetric types. Šiljak[9] also notes that if the applicability conditions of Popov[7] are not satisfied, use of these methods may predict sustained oscillations that do not exist, or may fail to predict sustained oscillations that do exist. Bogoliubov and Mitropolsky[10] have investigated the nonlinear analysis of self-excited systems using harmonic balance methods. Morrison[11] discussed the close relationship between averaging methods and the two-variable expansion

Received 1 February 2001; presented as Paper 2001-1472 at the AIAA/ASME/ASCE/AHS/ASC 42nd Structures, Structural Dynamics, and Materials Conference and Exhibit, Seattle, WA, 16–19 April 2001; revision received 25 September 2001; accepted for publication 10 December 2001.

*Associate Technical Fellow, Structures Vibration Technology, Commercial Airplane Group, P.O. Box 3707, MS 67-HL. Senior Member AIAA.

procedure.[12,13] Generalization of the two-variable expansion procedure using multiple-timescales and the validity of the asymptotic expansion method were discussed by Nayfeh.[14] Applications of averaging techniques and the multiple-timescale method to free, forced, and self-excited vibration problems with a variety of nonlinearities, including those having relay characteristics, were given by Nayfeh[15] and Nayfeh and Mook.[16]

The goal of this paper is to obtain a perturbation solution of the nonlinear shimmy equations for models with coulomb friction and freeplay that is valid in the neighborhood of a given equilibrium point. The method of multiple-timescales is applied to general autonomous self-excited systems to obtain expressions for the limit-cycle amplitude and frequency, and associated stability criteria. The approach follows that given by Morino,[17] Kuo et al.,[18] and Smith and Morino[19] for the analysis of nonlinear panel flutter in systems with quadratic and cubic nonlinearities and by Gordon and Merchant[4] to nonlinear shimmy models with velocity squared damping.

II. Problem Formulation

The equations of motion for the nonlinear shimmy models considered here (Appendix A) have the following general form when expressed in state variable representation:

$$\boldsymbol{M}\dot{\boldsymbol{q}} + \boldsymbol{K}\boldsymbol{q} = \hat{\boldsymbol{F}}_j \operatorname{sgn}(q_j) + \hat{\boldsymbol{F}}_k(\hat{F}_{\text{fp}}, q_k) \tag{1}$$

where

$$\operatorname{sgn}(q_j) = \begin{cases} +1, & q_j > 0 \\ 0, & q_j = 0 \quad \text{or} \quad |q_k| < \theta_{\text{fp}} \\ -1, & q_j < 0 \end{cases} \tag{2}$$

$$\hat{F}_{\text{fp}} = \begin{cases} -k_\theta \theta_{\text{fp}}, & q_k > +\theta_{\text{fp}} \\ -k_\theta q_k, & |q_k| \le +\theta_{\text{fp}} \\ +k_\theta \theta_{\text{fp}}, & q_k < -\theta_{\text{fp}} \end{cases} \tag{3}$$

$$\boldsymbol{K} = \boldsymbol{K}(V) \tag{4}$$

$\boldsymbol{M}$ and $\boldsymbol{K}$ are matrices for inertia and viscous damping and for stiffness, respectively, for the linear system about an equilibrium point $\boldsymbol{q}_e$ when the equations of motion are expressed in terms of the state variable vector $\boldsymbol{q}$. A dot over a symbol indicates differentiation with respect to time τ.

The vector $\hat{\boldsymbol{F}}_j \operatorname{sgn}(q_j)$ represents nonlinear terms due to coulomb friction between the oleo struts, where $\hat{\boldsymbol{F}}_j$ is a vector with constant components.

The vector $\hat{\boldsymbol{F}}_k = \hat{\boldsymbol{F}}_k(\hat{F}_{\text{fp}}, q_k)$ is a nonlinear function of q_k representing terms due to structural freeplay in the landing gear's torque links. The structural moment F_{fp} about the pivot, including freeplay effects, is given by

$$F_{\text{fp}} = k_\theta q_k + \hat{F}_{\text{fp}} \tag{5}$$

where k_θ is the torsional stiffness of the gear, or the torque links, depending on the particular structural model being used. $\hat{F}_{\text{fp}}$, which is given by Eq. (3), is a function of q_k and the torsional freeplay θ_{fp}. The linear term $k_\theta q_k$ in F_{fp} (which is assumed to be a function of $q_k = \theta$ here for simplicity only) is included in $\boldsymbol{K}$ (Appendix A).

V is a system parameter that is taken herein to be the ground speed of the aircraft. There is a critical value $V = V_0$ such that the linear system ($\hat{\boldsymbol{F}}_j = \hat{\boldsymbol{F}}_k = \boldsymbol{0}$) is stable for $V < V_0$ and unstable for $V > V_0$. For $V = V_0$, there is one pair of purely imaginary eigenvalues; all other eigenvalues have negative real parts. Thus, undamped harmonic oscillations occur for $V = V_0$. The periodic solution of Eq. (1) is sought in the local neighborhood of V_0 for small perturbations about the equilibrium point $\boldsymbol{q}_e = \boldsymbol{0}$. The vibration amplitudes are assumed to be high enough to engage the torque links, that is, $q_k \ge \theta_{\text{fp}}$.

Assume that V can be expanded as a power series in a small parameter ϵ about the critical point V_0 associated with a given equilibrium point $\boldsymbol{q}_e$,

$$V = V_0 + \epsilon V_1 + \epsilon^2 V_2 + \mathcal{O}(\epsilon^3) \tag{6}$$

The coefficients V_i are known constants, and V_0 defines the neutral stability point for the linear system, that is, one pair of eigenvalues for the linear system are imaginary. This implies that

$$\boldsymbol{K} = \boldsymbol{K}^{(0)}(V_0) + \epsilon \boldsymbol{K}^{(1)}(V_1) + \mathcal{O}(\epsilon^2) \tag{7}$$

Now rescale the nonlinear terms $\hat{\boldsymbol{F}}_j$ and $\hat{\boldsymbol{F}}_k$ that appear on the right-hand side of Eq. (1) by a factor of ϵ, where ϵ is a small parameter:

$$\hat{\boldsymbol{F}}_j = \epsilon \boldsymbol{F}_j \tag{8}$$

$$\hat{\boldsymbol{F}}_k = \epsilon \boldsymbol{F}_k \tag{9}$$

This choice of rescaling implies that the nonlinear terms $\hat{\boldsymbol{F}}_j$ and $\hat{\boldsymbol{F}}_k$ are of the same order of magnitude as changes in the linear term $\boldsymbol{K}(V)$ due to $(V - V_0)$. Then, Eq. (1) becomes

$$\boldsymbol{M}\dot{\boldsymbol{q}} + \boldsymbol{K}\boldsymbol{q} = \epsilon[\boldsymbol{F}_j \operatorname{sgn}(q_j) + \boldsymbol{F}_k] \tag{10}$$

With the use of the method of multiple timescales,[16] assume that there exists a uniformly valid asymptotic expansion for the dependent variables $\boldsymbol{q}$ of the form

$$\boldsymbol{q} = \sum_{m=0}^{M} \epsilon^m \boldsymbol{q}_m \tag{11}$$

Define multiple timescales τ_m such that

$$\tau_m = \epsilon^m \tau \tag{12}$$

where $m = 0, 1, 2, \ldots, M$. Then,

$$\frac{\mathrm{d}}{\mathrm{d}\tau} = \sum_{m=0}^{M} \epsilon^m \frac{\partial}{\partial \tau_m} + \mathcal{O}(\epsilon^{M+1}) \tag{13}$$

$$\frac{\mathrm{d}\boldsymbol{q}}{\mathrm{d}\tau} = \frac{\partial \boldsymbol{q}_0}{\partial \tau_0} + \epsilon\left[\frac{\partial \boldsymbol{q}_0}{\partial \tau_1} + \frac{\partial \boldsymbol{q}_1}{\partial \tau_0}\right] + \epsilon^2\left[\frac{\partial \boldsymbol{q}_2}{\partial \tau_0} + \frac{\partial \boldsymbol{q}_1}{\partial \tau_1} + \frac{\partial \boldsymbol{q}_0}{\partial \tau_2}\right] + \mathcal{O}(\epsilon^3) \tag{14}$$

Substitution of Eqs. (6) and (7) and (11–14) into Eq. (10) and collection of terms in powers of ϵ gives the following sets of equations to $\mathcal{O}(\epsilon^2)$.

For the ϵ^0-order system:

$$\boldsymbol{L}\boldsymbol{q}_0 = \boldsymbol{0} \tag{15}$$

where

$$\boldsymbol{L} = \boldsymbol{M}\frac{\partial}{\partial \tau_0} + \boldsymbol{K}^{(0)} \tag{16}$$

For the ϵ^1-order system:

$$\boldsymbol{L}\boldsymbol{q}_1 = -\boldsymbol{K}^{(1)}\boldsymbol{q}_0 - \boldsymbol{M}\frac{\partial \boldsymbol{q}_0}{\partial \tau_1} + \boldsymbol{F}_j(V_0, \boldsymbol{q}_0) \operatorname{sgn}(q_{j0}) + \boldsymbol{F}_k(V_0, \boldsymbol{q}_0) \tag{17}$$

III. Problem Solution

A. ϵ^0-Order Solution

The ϵ_0-order system in Eq. (15) is the set of linear shimmy equations for small perturbations about the equilibrium point $\boldsymbol{q}_e = \boldsymbol{0}$. At some critical value of the parameter $V = V_0$, one pair of eigenvalues are purely imaginary and all other eigenvalues have negative real parts. Thus, undamped harmonic oscillations occur for V_0. The harmonic solution to Eq. (15) for $\boldsymbol{q}_0$ is

$$\boldsymbol{q}_0 = A\boldsymbol{u}e^{i\psi} + A\boldsymbol{u}^* e^{-i\psi} = 2A \operatorname{Re}[\boldsymbol{u}e^{i\psi}] \tag{18}$$

where $i = \sqrt{-1}$, and A is a real quantity that is a function of the timescales τ_m, $\boldsymbol{u}$ is a complex eigenvector, and $\boldsymbol{u}^*$ is the complex conjugate of $\boldsymbol{u}$. Here,

$$\psi = \omega_0 \tau_0 + \phi(\tau_1, \tau_2, \ldots) \tag{19}$$

$$A = A(\tau_1, \tau_2, \ldots) \tag{20}$$

Substitution of Eqs. (18) and (19) into Eq. (15) yields

$$\boldsymbol{L}_0 \boldsymbol{u} = \boldsymbol{0} \tag{21}$$

where

$$\boldsymbol{L}_0 = i\omega_0 \boldsymbol{M} + \boldsymbol{K}^{(0)} \tag{22}$$

and $\boldsymbol{K}^{(0)}$ is a function of the system parameter V_0. Equation (21) possesses nontrivial solutions if and only if

$$\det \boldsymbol{L}_0 = 0 \tag{23}$$

For $V = V_0$, the requirement in Eq. (23) determines the eigenvalue ω_0, the shimmy frequency for the linear system. Hence, the eigenvector $\boldsymbol{u}$ associated with ω_0 can be obtained.

B. ϵ^1-Order Solution

Expand the nonlinear terms due to coulomb friction $\boldsymbol{F}_j \operatorname{sgn}(q_{j0})$ and structural freeplay $\boldsymbol{F}_k$ that appear on the right-hand side of Eq. (17) in complex Fourier series with

$$\boldsymbol{f}_j^{(n)} = \frac{1}{2\pi} \int_0^{2\pi} \boldsymbol{F}_j \operatorname{sgn}(q_{j0}) e^{-in\psi} \, \mathrm{d}\psi \tag{24}$$

$$\boldsymbol{f}_k^{(n)} = \frac{1}{2\pi} \int_0^{2\pi} \boldsymbol{F}_k e^{-in\psi} \, \mathrm{d}\psi \tag{25}$$

for $-\infty \le n \le +\infty$, and where

$$q_{j0} = 2A \operatorname{Re}\left[u_j e^{i\psi}\right] \tag{26}$$

Now substitute $\boldsymbol{q}_0$ from Eq. (18) into Eqs. (17), (24), and (25) to obtain an equation for $\boldsymbol{q}_1$:

$$\begin{aligned} \boldsymbol{L}\boldsymbol{q}_1 = \sum_{-\infty < n < +\infty}^{n \neq \pm 1} & \left[\boldsymbol{f}_j^{(n)} + \boldsymbol{f}_k^{(n)}(A)\right] e^{in\psi} + \left[\boldsymbol{f}_j^{(+1)} + \boldsymbol{f}_k^{(+1)}(A) \right. \\ & \left. + \boldsymbol{K}^{(1)} \boldsymbol{u} A\right] e^{+i\psi} + \left(\frac{\partial A}{\partial \tau_1} + iA \frac{\partial \psi}{\partial \tau_1}\right) \boldsymbol{M}\boldsymbol{u} e^{+i\psi} + \left[\boldsymbol{f}_j^{(-1)} \right. \\ & \left. + \boldsymbol{f}_k^{(-1)}(A) + \boldsymbol{K}^{(1)} \boldsymbol{u}^* A\right] e^{-i\psi} + \left(\frac{\partial A}{\partial \tau_1} - iA \frac{\partial \psi}{\partial \tau_1}\right) \boldsymbol{M}\boldsymbol{u}^* e^{-i\psi} \end{aligned} \tag{27}$$

The terms on the right-hand side of Eq. (27) that multiply $e^{+i\psi}$ and $e^{-i\psi}$ are secular and lead to spurious resonance because the homogeneous solution is

$$\boldsymbol{q}_1 = B\boldsymbol{u} e^{+i\psi} + B\boldsymbol{u}^* e^{-i\psi} \tag{28}$$

From matrix theory, this spurious resonance can be suppressed by requiring that

$$\boldsymbol{v}^T \left[\boldsymbol{f}_j^{(+1)} + \boldsymbol{f}_k^{(+1)}(A) + \boldsymbol{K}^{(1)} \boldsymbol{u} A\right] + \boldsymbol{v}^T \left(\frac{\partial A}{\partial \tau_1} + iA \frac{\partial \psi}{\partial \tau_1}\right) \boldsymbol{M}\boldsymbol{u} = 0 \tag{29}$$

or

$$\left(\frac{\partial A}{\partial \tau_1} + iA \frac{\partial \psi}{\partial \tau_1}\right) + \beta A + \gamma + \delta = 0 \tag{30}$$

where

$$\alpha = \boldsymbol{v}^T \boldsymbol{M} \boldsymbol{u} \tag{31}$$

$$\beta = \boldsymbol{v}^T \boldsymbol{K}^{(1)} \boldsymbol{u} \Big/ \alpha \tag{32}$$

$$\gamma = \boldsymbol{v}^T \boldsymbol{f}_j^{(+1)} \Big/ \alpha \tag{33}$$

$$\delta = \boldsymbol{v}^T \boldsymbol{f}_k^{(+1)} \Big/ \alpha \tag{34}$$

where $\boldsymbol{v}$ is the left eigenvector associated with

$$\boldsymbol{v}^T \boldsymbol{L}_0 = \boldsymbol{0}^T \tag{35}$$

or

$$\boldsymbol{L}_0^T \boldsymbol{v} = \boldsymbol{0} \tag{36}$$

where $\boldsymbol{L}_0$ is defined in Eq. (22). When the real and imaginary parts in Eq. (30) are equated to zero individually, partial differential equations are obtained for the amplitude A and phase ψ, namely,

$$\frac{\partial A}{\partial \tau_1} + \beta_R A + \gamma_R + \delta_R = 0 \tag{37}$$

$$\left(\frac{\partial \psi}{\partial \tau_1} + \beta_I\right) A + \gamma_I + \delta_I = 0 \tag{38}$$

C. $\mathcal{O}(\epsilon^1)$ Limit-Cycle Solution

For stationary periodic motion, $\partial A / \partial \tau_1 = 0$, and from Eq. (37), an equation for the limit-cycle solution $G(A = A_{\mathrm{LC}}) = 0$ is obtained:

$$G(A) = \beta_R A + \gamma_R + \delta_R = 0 \tag{39}$$

When Eqs. (11) and (18–20) are combined with $\epsilon = (V - V_0)/V_1$, an approximation for the limit cycle is obtained:

$$\boldsymbol{q} = 2A_{\mathrm{LC}} \operatorname{Re}[\boldsymbol{u} e^{i\omega\tau_0}] + \mathcal{O}(\epsilon) \tag{40}$$

For the general case considered in Eq. (39), $\gamma = \gamma(A)$ is determined by the coulomb friction terms from Eqs. (24) and (33); α is given by Eq. (31), β is a function of $\boldsymbol{K}^{(1)}(V_1)$ that is determined from Eq. (32), and $\delta = \delta(A)$ is determined by the structural freeplay-dependent terms from Eqs. (25) and (34). Note that β, γ, and δ are functions dependent on the normalized forms of $\boldsymbol{u}$ and $\boldsymbol{v}$.

The phase $\psi = \omega\tau_0$, where ω is the nonlinear frequency, is determined from Eqs. (19) and (38)

$$\psi = \omega_0 \tau_0 - \epsilon[\beta_I + (\gamma_I + \delta_I)/A_{\mathrm{LC}}]\tau_0 \tag{41}$$

with the limit-cycle amplitude $2A = 2A_{\mathrm{LC}}$ being determined from Eq. (39) and $\epsilon = (V - V_0)/V_1$ with $V_1 = +1$ for $V > V_0$ and $V_1 = -1$ for $V < V_0$. Alternatively, one can choose $\epsilon = 1$ with $V = V_0 + V_1$, and $V_1 > 0$ for $V > V_0$, and $V_1 < 0$ for $V < V_0$.

IV. Nonlinear Stability Analysis

A. Coulomb Friction Only

Consider Eq. (1) when no nonlinear terms due to freeplay are present, that is, $\hat{\boldsymbol{F}}_k = \boldsymbol{0}$. Then, $\delta = 0$ in Eq. (30) and Eqs. (37) and (38) for the amplitude A and phase ψ, respectively, become

$$\frac{\partial A}{\partial \tau_1} + \beta_R A + \gamma_R = 0 \tag{42}$$

$$\left(\frac{\partial \psi}{\partial \tau_1} + \beta_I\right) A + \gamma_I = 0 \tag{43}$$

Here, γ_R and γ_I are constants determined by Eqs. (24) and (33). The solution of Eq. (42) is

$$A = K(\tau_2, \tau_3, \ldots) e^{-\beta_R \tau_1} - (\gamma_R / \beta_R) \tag{44}$$

where $A(\tau_1 = 0) = A_0$ and $K = (A_0 + \gamma_R/\beta_R)$. Hence,

$$A = (A_0 + \gamma_R/\beta_R)e^{-\beta_R \tau_1} - \gamma_R/\beta_R \tag{45}$$

where $\tau_1 = \epsilon\tau_0$ and $\epsilon = (V - V_0)/V_1$.

1. $\gamma_R > 0$ and $V < V_0$

Consider the case $\gamma_R > 0$ for $V < V_0$. Because the linear system is stable, $\beta_R > 0$. Hence, $(\gamma_R/\beta_R) > 0$. Also $(A_0 + \gamma_R/\beta_R) > 0$ for $A_0 > -\gamma_R/\beta_R$. Because $\beta_R > 0$, then $e^{-\beta_R\tau_1} \to 0$ as $\tau_1 \to \infty$. Thus, the system is stable regardless of the magnitude or sign of A_0 for $V < V_0$.

2. $\gamma_R > 0$ and $V > V_0$

Consider the case $\gamma_R > 0$ for $V > V_0$. Here, $\beta_R < 0$ because the linear system is unstable, and hence, $(\gamma_R/\beta_R) < 0$. For $A_0 \le |\gamma_R/\beta_R|$, then $(A_0 + \gamma_R/\beta_R) < 0$. Thus, $A \to 0$ at a particular $\tau_1 = \tau_{10}$ and for $\tau_1 \to \infty$. For $A_0 > |\gamma_R/\beta_R|$, then $(A_0 + \gamma_R/\beta_R) > 0$, and $A \to \infty$ as $\tau_1 \to \infty$. Hence, an unstable limit cycle exists for $V > V_0$.

3. $\gamma_R < 0$ and $V < V_0$

Consider the case $\gamma_R < 0$ for $V < V_0$. Because the linear system is stable, $\beta_R > 0$. Hence, $(\gamma_R/\beta_R) < 0$. Also $(A_0 + \gamma_R/\beta_R) < 0$ for $A_0 \le |\gamma_R/\beta_R|$. Because $\beta_R > 0$, then $e^{-\beta_R\tau_1} \to 0$ as $\tau_1 \to \infty$. Thus, $A \to (-\gamma_R/\beta_R)$ as $\tau_1 \to \infty$. Hence, a stable limit cycle exists for $V < V_0$.

4. $\gamma_R < 0$ and $V > V_0$

Consider the case $\gamma_R < 0$ for $V > V_0$. Here, $\beta_R < 0$ because the linear system is unstable, and hence, $(\gamma_R/\beta_R) > 0$. For $A_0 \le |\gamma_R/\beta_R|$, then $(A_0 + \gamma_R/\beta_R) > 0$. For $A_0 > |\gamma_R/\beta_R|$, then $(A_0 + \gamma_R/\beta_R) > 0$. Thus, $A \to \infty$ as $\tau_1 \to \infty$. Therefore, the system is unstable regardless of the magnitude or sign of A_0 for $V > V_0$.

5. Limit-Cycle Solution

For $\partial A/\partial\tau_1 = 0$, there is one stationary solution to Eq. (42), $A = |-\gamma_R/\beta_R|$, which corresponds to a limit cycle. When Eqs. (11) and (18–20) are combined with $\epsilon = (V - V_0)/V_1$, an approximation for the limit cycle is obtained:

$$\boldsymbol{q} = 2|\gamma_R/\beta_R|\,\mathrm{Re}[\boldsymbol{u}e^{i\omega\tau_0}] + \mathcal{O}(\epsilon) \tag{46}$$

where the frequency ω is given by

$$\omega = \omega_0 + |V - V_0|[-\beta_I + \gamma_I(\beta_R/\gamma_R)] + \mathcal{O}(\epsilon) \tag{47}$$

Thus, depending on the stability of the singular point near $V = V_0$, there are four possible scenarios for the qualitative behaviour of the limit cycles. Here, it has been assumed that the linear system is stable (unstable) for $V < V_0 (V > V_0)$ and that for $V = V_0$ one pair of eigenvalues is purely imaginary. In this situation, when $\gamma_R > 0$, an unstable limit cycle exits for $V > V_0$ and the system is stable for $V < V_0$; when $\gamma_R < 0$, a stable limit cycle exits for $V < V_0$ and the system is unstable for $V > V_0$. For the situation where the linear system is unstable (stable) for $V < V_0 (V > V_0)$ with one pair of eigenvalues purely imaginary at $V = V_0$, the qualitative behavior of the limit cycles is simply the reverse of that just described.

B. Torsional Freeplay Only

Consider Eq. (30) when nonlinear terms due to coulomb friction are not present, that is, $\boldsymbol{F}_j = \boldsymbol{f}_j^{(n)} = \boldsymbol{0}$. Then, $\gamma = 0$ and Eqs. (37) and (38) for the amplitude A and phase ψ, respectively, become

$$\frac{\partial A}{\partial \tau_1} + \beta_R A + \delta_R = \frac{\partial A}{\partial \tau_1} + G(A) = 0 \tag{48}$$

$$\left(\frac{\partial \psi}{\partial \tau_1} + \beta_I\right) A + \delta_I = 0 \tag{49}$$

For $\partial A/\partial\tau_1 = 0$, there is one stationary solution of Eq. (48), $A = A_{\mathrm{LC}}$, which corresponds to a limit cycle. When Eqs. (11) and (18–20) are combined with $\epsilon = (V - V_0)/V_1$, an approximation for the limit cycle is obtained.

$$\boldsymbol{q} = 2A_{\mathrm{LC}}\,\mathrm{Re}[\boldsymbol{u}e^{i\omega\tau_0}] + \mathcal{O}(\epsilon) \tag{50}$$

where the frequency ω is given by

$$\omega = \omega_0 + |V - V_0|(-\beta_I - \delta_I/A_{\mathrm{LC}}) + \mathcal{O}(\epsilon) \tag{51}$$

Stability of the limit cycle is determined by evaluation of $G'(A) = \mathrm{d}G/\mathrm{d}A$, where $G(A) = \beta_R A + \delta_R$, at the singular point $A = A_{\mathrm{LC}}$. The limit cycle is stable for $G'(A_{\mathrm{LC}}) > 0$ and unstable for $G'(A_{\mathrm{LC}}) < 0$.

C. Freeplay and Coulomb Friction

Consider the case when nonlinear terms due to torsional freeplay and coulomb friction are present, that is, $\gamma \neq 0$ and $\delta \neq 0$ in Eq. (30). Then, the amplitude A and phase ψ are given by Eqs. (37) and (38), respectively.

For stationary periodic motion, $\partial A/\partial\tau_1 = 0$, and from Eq. (37), the equation for the limit-cycle amplitude $G(A) = G(A_{\mathrm{LC}}) = 0$ is obtained, that is, Eq. (39). The phase angle ψ is given by Eq. (41).

Stability of the limit cycle is determined by evaluation of $G'(A) = \mathrm{d}G/\mathrm{d}A$, where $G(A) = \beta_R A + \gamma_R + \delta_R$, at the singular point $A = A_{\mathrm{LC}}$. The limit cycle is stable for $G'(A_{\mathrm{LC}}) > 0$ and unstable for $G'(A_{\mathrm{LC}}) < 0$.

V. Numerical Examples

As an application of the preceding analysis, a simple shimmy model with nonlinear terms representing coulomb friction between the strut oleos and freeplay in the torque links is examined. The model, described in Appendix A, is a modification of one studied by Nybakken.[20] The solution of Eq. (1) is obtained in the local neighborhood of V_0 for small perturbations about the equilibrium point $\boldsymbol{q}_e = \boldsymbol{0}$. The perturbation solutions are compared with ones obtained by numerical integration using a variable-step Runge–Kutta algorithm[21] and a time step $\Delta t = 1.0 \times 10^{-5}$ s. The parameter values used for these calculations are given in Appendix B. For the perturbation solution, subroutine HDZAFS,[22] which employs Jarratt's method, is used to find the real roots of the amplitude equation $G(A_{\mathrm{LC}}) = 0$.

A. Coulomb Friction Only

For the shimmy model described in Appendix A with coulomb friction but no freeplay present, the equations of motion are

$$\boldsymbol{M}\dot{\boldsymbol{q}} + \boldsymbol{K}\boldsymbol{q} = \hat{\boldsymbol{F}}_1\,\mathrm{sgn}(q_1) \tag{52}$$

where

$$\boldsymbol{q} = \{q_1 \quad q_2 \quad q_3\}^T = \{\dot{\theta} \quad \theta \quad y\}^T \tag{53}$$

$$\boldsymbol{M} = \begin{bmatrix} I_\theta & C_\theta & 0 \\ 0 & 0 & \lambda \\ 0 & 1 & 0 \end{bmatrix} \tag{54}$$

$$\boldsymbol{K} = \begin{bmatrix} 0 & k_1 & k_3 \\ 0 & k_4 V & V \\ -1 & 0 & 0 \end{bmatrix} \tag{55}$$

$$\mathrm{sgn}(q_1) = \begin{cases} +1, & q_1 > 0 \\ 0, & q_1 = 0 \\ -1, & q_1 < 0 \end{cases} \tag{56}$$

$$\hat{\boldsymbol{F}}_1 = \hat{\boldsymbol{F}}_{\mathrm{cf}} = -\{C_{\mathrm{cf}} \quad 0 \quad 0\}^T \tag{57}$$

Then

$$\boldsymbol{K}^{(0)} = \begin{bmatrix} 0 & k_1 & k_3 \\ 0 & k_4 V_0 & V_0 \\ -1 & 0 & 0 \end{bmatrix} \tag{58}$$

$$\boldsymbol{K}^{(1)} = \begin{bmatrix} 0 & 0 & 0 \\ 0 & k_4 V_1 & V_1 \\ 0 & 0 & 0 \end{bmatrix} \tag{59}$$

For the linear system (ϵ^0 order), Eq. (23) gives the shimmy speed V_0 and frequency ω_0,

$$V_0^2 + V_0(\lambda C_\theta / I_\theta + k_3 k_4 \lambda / C_\theta) + k_1 \lambda^2 \big/ I_\theta = 0 \tag{60}$$

$$\omega_0^2 = (\lambda k_\theta + C_\theta V_0)/(I_\theta \lambda) \tag{61}$$

The right and left eigenvectors $\boldsymbol{u}$ and $\boldsymbol{v}$ corresponding to ω_0 and V_0 are determined from Eqs. (21) and (36), respectively. Here, $\boldsymbol{u}$ has been normalized so that $q_{20} = 2A \cos\psi$.

$$\boldsymbol{u} = \begin{Bmatrix} i\omega_0 \\ 1 \\ -k_4 V_0/(V_0 + i\lambda\omega_0) \end{Bmatrix} \tag{62}$$

$$\boldsymbol{v} = \begin{Bmatrix} 1 \\ -k_3/(V_0 + i\lambda\omega_0) \\ i I_\theta \omega_0 \end{Bmatrix} \tag{63}$$

Here, α, β, γ and are computed using Eqs. (31–33) and (62) and (63):

$$\alpha = \alpha_R + i\alpha_I \tag{64}$$

$$\alpha_R = C_\theta + \frac{\lambda k_3 k_4 V_0 \left(V_0^2 - \lambda^2 \omega_0^2\right)}{\left(V_0^2 + \lambda^2 \omega_0^2\right)^2} \tag{65}$$

$$\alpha_I = 2 I_\theta \omega_0 - \frac{2 k_3 k_4 V_0^2 \lambda^2 \omega_0}{\left(V_0^2 + \lambda^2 \omega_0^2\right)^2} \tag{66}$$

$$\beta = \frac{V_1 k_3 k_4 \left[-2\lambda^2 V_0 \omega_0^2 + i\left(\lambda^3 \omega_0^3 - \lambda \omega_0 V_0^2\right)\right]}{\alpha\left(V_0^2 + \lambda^2 \omega_0^2\right)^2} \tag{67}$$

$$\gamma = \gamma_R + i\gamma_I = \frac{2 i C_{\mathrm{cf}}}{\pi \epsilon \alpha} \tag{68}$$

$$\gamma_R = \frac{2 C_{\mathrm{cf}}}{\pi \epsilon} \frac{\alpha_I}{\left(\alpha_R^2 + \alpha_I^2\right)} \tag{69}$$

$$\gamma_I = \frac{2 C_{\mathrm{cf}}}{\pi \epsilon} \frac{\alpha_R}{\left(\alpha_R^2 + \alpha_I^2\right)} \tag{70}$$

$$\epsilon = \frac{V - V_0}{V_1} \tag{71}$$

The limit-cycle amplitude $2A_{\mathrm{LC}} = 2|\gamma_R/\beta_R|$ is given by Eq. (46) and the frequency by Eq. (47). Note that the limit-cycle amplitude is inversely proportional to $\epsilon = (V - V_0)/V_1$ and that the nonlinear frequency ω is proportional to ϵ.

A plot of limit-cycle amplitude θ vs nondimensional ground speed for $C_{\mathrm{cf}} = 100$ lb · in. (11.298 N · m) and no freeplay that compares results from the perturbation solution with those from direct numerical integration of the nonlinear equations is presented in Fig. 1. Also given in Fig. 1 are frequencies obtained by the perturbation and numerical integration solutions.

For ground speeds less than V_0, that is, speed ratios $V/V_0 < 1$, the system is stable. For speeds $V > V_0$, that is speed ratios $V/V_0 > 1$, an unstable limit cycle exists. In this region, for an initial amplitude greater than the limit-cycle amplitude shown at a given speed ratio, that is, ground speed, the system is unstable; for an initial amplitude less than this value, the system is stable, and the response will decay. For speeds $V > V_0$, as the taxi speed approaches the critical value V_0, the shimmy speed for the linear system, the frequency approaches the linear shimmy frequency ω_0 and the amplitude increases rapidly.

Both the amplitudes and frequencies determined by the perturbation solution are seen to be in excellent agreement with those from the numerical integration solution. For example, at a ground speed ratio $V/V_0 = 1.83$, the amplitude predicted by the perturbation solution is about 15.5% lower than that obtained from numerical integration. (The frequency is about 2.9% lower.) For a ground speed ratio of $V/V_0 = 1.22$, the difference between the amplitudes is about 5.4%. (The frequency is about 1.8% lower.) At a speed ratio of $V/V_0 = 1.07$, the difference is less than 2.6%. (The frequency is less than 1.8% lower.)

B. Torsional Freeplay Only

For the shimmy model described in Appendix A with freeplay but no coulomb friction present, the equations of motion are

$$\boldsymbol{M}\dot{\boldsymbol{q}} + \boldsymbol{K}\boldsymbol{q} = \hat{\boldsymbol{F}}_2 \tag{72}$$

where

$$\boldsymbol{q} = \{q_1 \quad q_2 \quad q_3\}^T = \{\dot{\theta} \quad \theta \quad y\}^T \tag{73}$$

$$\boldsymbol{M} = \begin{bmatrix} I_\theta & C_\theta & 0 \\ 0 & 0 & \lambda \\ 0 & 1 & 0 \end{bmatrix} \tag{74}$$

$$\boldsymbol{K} = \begin{bmatrix} 0 & k_1 & k_3 \\ 0 & k_4 V & V \\ -1 & 0 & 0 \end{bmatrix} \tag{75}$$

$$\hat{\boldsymbol{F}}_2 = \hat{\boldsymbol{F}}_{\mathrm{fp}} = -\{\hat{F}_{\mathrm{fp}} \quad 0 \quad 0\}^T \tag{76}$$

$$\hat{F}_{\mathrm{fp}} = \begin{cases} -k_\theta \theta_{\mathrm{fp}}, & \theta > +\theta_{\mathrm{fp}} \\ -k_\theta \theta, & |\theta| \le +\theta_{\mathrm{fp}} \\ +k_\theta \theta_{\mathrm{fp}}, & \theta < -\theta_{\mathrm{fp}} \end{cases} \tag{77}$$

Then,

$$\boldsymbol{K}^{(0)} = \begin{bmatrix} 0 & k_1 & k_3 \\ 0 & k_4 V_0 & V_0 \\ -1 & 0 & 0 \end{bmatrix} \tag{78}$$

$$\boldsymbol{K}^{(1)} = \begin{bmatrix} 0 & 0 & 0 \\ 0 & k_4 V_1 & V_1 \\ 0 & 0 & 0 \end{bmatrix} \tag{79}$$

For the linear system (ϵ^0 order), Eq. (23) gives the shimmy speed V_0 and frequency ω_0:

$$V_0^2 + V_0(\lambda C_\theta / I_\theta + k_3 k_4 \lambda / C_\theta) + k_1 \lambda^2 \big/ I_\theta = 0 \tag{80}$$

$$\omega_0^2 = (\lambda k_\theta + C_\theta V_0)/(I_\theta \lambda) \tag{81}$$

The right and left eigenvectors $\boldsymbol{u}$ and $\boldsymbol{v}$ corresponding to ω_0 and V_0 are determined from Eqs. (21) and (36), respectively. Here, $\boldsymbol{u}$ is normalized so that $q_{20} = 2A \sin\psi$ and, thus, $\delta = 0$ when $\theta_{\mathrm{fp}} = 0$,

$$\boldsymbol{u} = \begin{Bmatrix} +\omega_0 \\ -i \\ i k_4 V_0/(V_0 + i\lambda\omega_0) \end{Bmatrix} \tag{82}$$

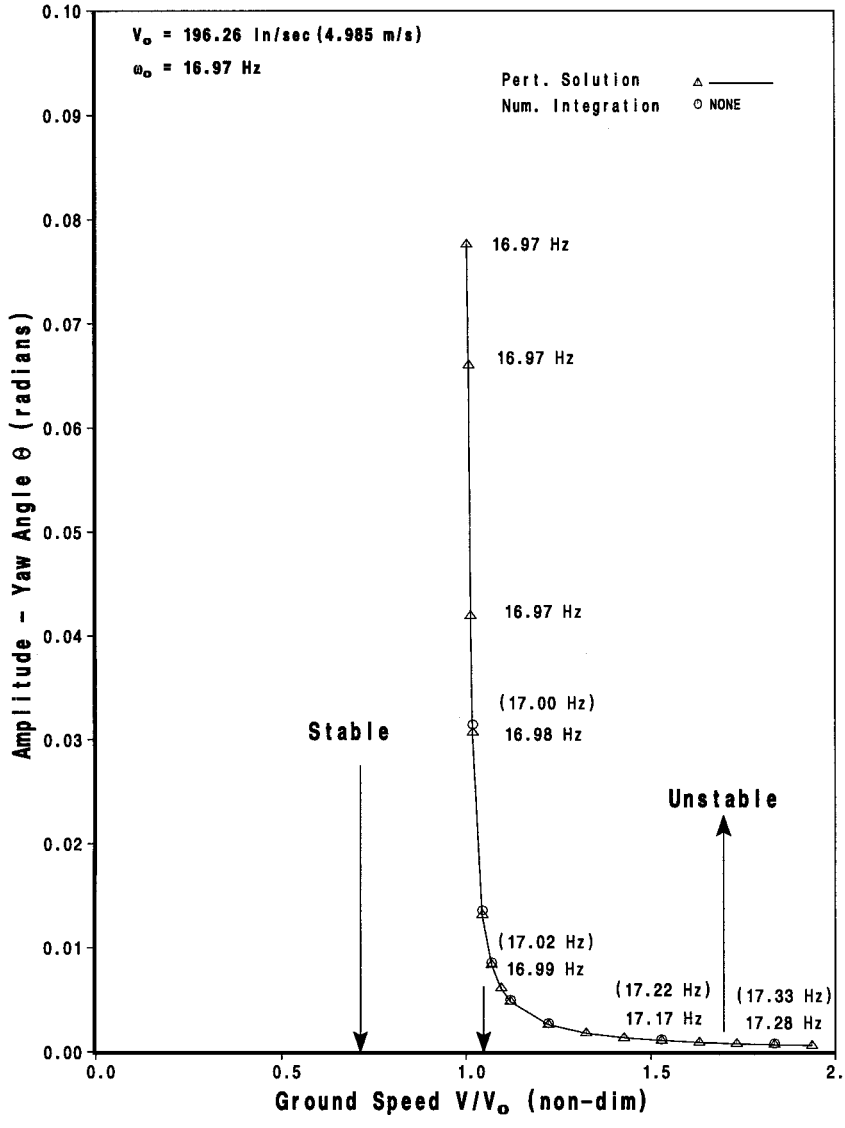

Fig. 1 Limit-cycle amplitude vs taxi speed: $C_{cf} = 100$ lb · in. and $\theta_{fp} = 0$.

$$\boldsymbol{v} = \begin{Bmatrix} 1 \\ -k_3/(V_0 + i\lambda\omega_0) \\ iI_\theta\omega_0 \end{Bmatrix} \tag{83}$$

Here, α, β, and δ are computed using Eqs. (31), (32), and (34) with Eqs. (82) and (83). Note that $\boldsymbol{u}$ has been normalized so that $q_{20} = 2A\sin\psi$. Also, $\theta_{fp} \le 2A$.

$$\alpha_I = -C_\theta - \frac{\lambda k_3 k_4 V_0\left(V_0^2 - \lambda^2\omega_0^2\right)}{\left(V_0^2 + \lambda^2\omega_0^2\right)^2} \tag{84}$$

$$\alpha_R = 2I_\theta\omega_0 - \frac{2k_3 k_4 V_0^2\lambda^2\omega_0}{\left(V_0^2 + \lambda^2\omega_0^2\right)^2} \tag{85}$$

$$\alpha = \alpha_R + i\alpha_I \tag{86}$$

$$\beta = \frac{V_1 k_3 k_4\left[\left(\lambda^3\omega_0^3 - \lambda\omega_0 V_0^2\right) + 2i\lambda^2 V_0\omega_0^2\right]}{\alpha\left(V_0^2 + \lambda^2\omega_0^2\right)^2} \tag{87}$$

$$\delta = \delta_R + i\delta_I \tag{88}$$

$$\delta_R = g_1 A\psi_{fp} + g_1\left(\frac{\theta_{fp}}{2}\right)\sqrt{1 - \left(\frac{\theta_{fp}}{2A}\right)^2} \tag{89}$$

$$\delta_I = g_2 A\psi_{fp} + g_2\left(\frac{\theta_{fp}}{2}\right)\sqrt{1 - \left(\frac{\theta_{fp}}{2A}\right)^2} \tag{90}$$

$$\psi_{fp} = \sin^{-1}\left(\frac{\theta_{fp}}{2A}\right) \tag{91}$$

$$g_1 = \frac{2k_\theta}{\pi\epsilon}\left(\frac{\alpha_I}{\alpha_R^2 + \alpha_I^2}\right) \tag{92}$$

$$g_2 = \frac{2k_\theta}{\pi\epsilon}\left(\frac{\alpha_R}{\alpha_R^2 + \alpha_I^2}\right) \tag{93}$$

$$\epsilon = \frac{V - V_0}{V_1} \tag{94}$$

The limit-cycle amplitude is given by $2A_{LC}$ from Eq. (48), where A_{LC} is the stationary solution of the amplitude equation when $\partial A/\partial\tau_1 = 0$, that is, the positive real roots of the

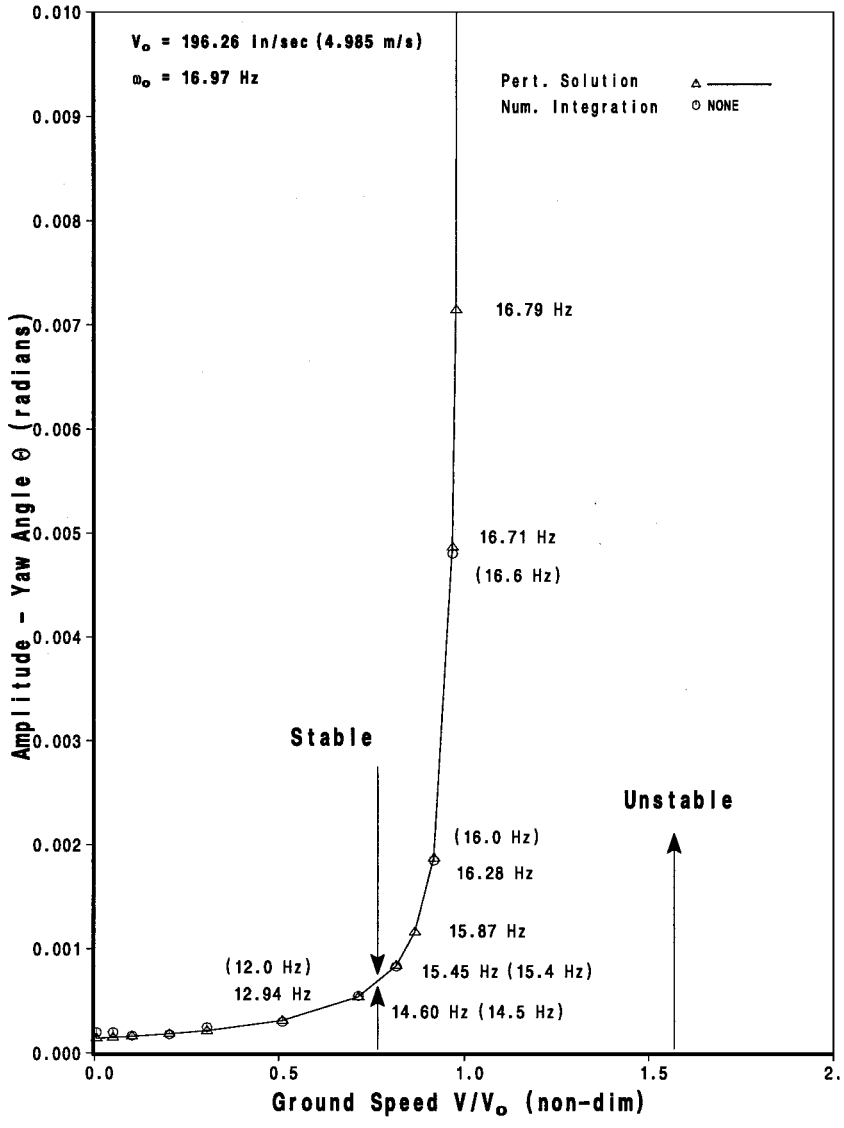

Fig. 2 Limit-cycle amplitude vs taxi speed: $C_{cf} = 0$ and $\theta_{fp} = 0.0001$ rad.

equation $G(A_{LC}) = 0$. The frequency is given by Eq. (51). A plot of limit-cycle amplitude θ vs nondimensional ground speed for $\theta_{fp} = 1.0 \times 10^{-4}$ rad and no coulomb friction that compares results from the perturbation solution with those from direct numerical integration of the nonlinear equations is presented in Fig. 2.

For ground speeds $V < V_0$, that is, speed ratios $V/V_0 < 1$, a stable limit cycle exists. In this region, for initial amplitudes either greater or less than the limit-cycle amplitude shown at a given speed ratio, that is, ground speed, the system is stable, and the initial response will decay to a stable limit-cycle oscillation. As the taxi speed approaches the critical value V_0, the shimmy speed for the linear system, the nonlinear frequency ω approaches the linear shimmy frequency ω_0 and the amplitude increases rapidly. For ground speeds higher than V_0, that is, speed ratios $V/V_0 > 1$, the system is unstable.

Both the amplitudes and frequencies determined by the perturbation solution are seen to be in excellent agreement with those from the numerical integration solution. For example, at a ground speed ratio $V/V_0 = 0.51$, the amplitude predicted by the perturbation solution is about 3.3% higher than that obtained from numerical integration. (The frequency is about 7.8% higher.) For a ground speed ratio of $V/V_0 = 0.92$, the difference between the amplitudes is about 1.1%. (The frequency is about 1.8% higher.) At a speed ratio of $V/V_0 = 0.97$, the difference between the amplitudes is less than 1.0%. (The frequency predicted by the perturbation solution is less than 0.25% higher.)

As the taxi speed approaches $V = 0$, there is a change in the response characteristic to a relaxation-type oscillation, and the frequency (not shown in Fig. 2) predicted by the perturbation solution does not agree nearly as well with that obtained by numerical integration, for example, 10.43 Hz vs 5.8 Hz at $V/V_0 = 0.2$, even though the amplitudes are still quite close. (The perturbation solution's amplitude is about 2.2% higher than that obtained by numerical integration at $V/V_0 = 0.2$.) The perturbation solution assumes that the frequency does not deviate too greatly from the value ω_0 associated with the critical speed V_0.

C. Coulomb Friction and Freeplay

For the shimmy model described in Appendix A with freeplay and coulomb friction present, the equations of motion are

$$\boldsymbol{M}\dot{\boldsymbol{q}} + \boldsymbol{K}\boldsymbol{q} = \hat{\boldsymbol{F}}_1 \operatorname{sgn}(q_1) + \hat{\boldsymbol{F}}_2 \tag{95}$$

where

$$\boldsymbol{q} = \{q_1 \quad q_2 \quad q_3\}^T = \{\dot{\theta} \quad \theta \quad y\}^T \tag{96}$$

$$\boldsymbol{M} = \begin{bmatrix} I_\theta & C_\theta & 0 \\ 0 & 0 & \lambda \\ 0 & 1 & 0 \end{bmatrix} \tag{97}$$

$$\boldsymbol{K} = \begin{bmatrix} 0 & k_1 & k_3 \\ 0 & k_4 V & V \\ -1 & 0 & 0 \end{bmatrix} \tag{98}$$

$$\begin{aligned} \operatorname{sgn}(q_1) = +1, &\qquad q_1 > 0 \\ 0, &\qquad q_1 = 0 \quad \text{or} \quad |q_2| < \theta_{\text{fp}} \\ -1, &\qquad q_1 < 0 \end{aligned} \tag{99}$$

$$\hat{\boldsymbol{F}}_1 = \hat{\boldsymbol{F}}_{\text{cf}} = -\{C_{\text{cf}} \quad 0 \quad 0\}^T \tag{100}$$

$$\hat{\boldsymbol{F}}_2 = \hat{\boldsymbol{F}}_{\text{fp}} = -\{\hat{F}_{\text{fp}} \quad 0 \quad 0\}^T \tag{101}$$

$$\begin{aligned} \hat{F}_{\text{fp}} = -k_\theta \theta_{\text{fp}}, &\qquad \theta > +\theta_{\text{fp}} \\ -k_\theta \theta, &\qquad |\theta| \le +\theta_{\text{fp}} \\ +k_\theta \theta_{\text{fp}}, &\qquad \theta < -\theta_{\text{fp}} \end{aligned} \tag{102}$$

Then,

$$\boldsymbol{K}^{(0)} = \begin{bmatrix} 0 & k_1 & k_3 \\ 0 & k_4 V_0 & V_0 \\ -1 & 0 & 0 \end{bmatrix} \tag{103}$$

$$\boldsymbol{K}^{(1)} = \begin{bmatrix} 0 & 0 & 0 \\ 0 & k_4 V_1 & V_1 \\ 0 & 0 & 0 \end{bmatrix} \tag{104}$$

For the linear system (ϵ^0 order), Eq. (23) gives the shimmy speed V_0 and frequency ω_0:

$$V_0^2 + V_0\left(\frac{\lambda C_\theta}{I_\theta} + \frac{k_3 k_4 \lambda}{C_\theta}\right) + \frac{k_1 \lambda^2}{I_\theta} = 0 \tag{105}$$

$$\omega_0^2 = \frac{\lambda k_\theta + C_\theta V_0}{I_\theta \lambda} \tag{106}$$

The right and left eigenvectors $\boldsymbol{u}$ and $\boldsymbol{v}$ corresponding to ω_0 and V_0 are determined from Eqs. (21) and (36), respectively. Here, $\boldsymbol{u}$ is normalized so that $q_{20} = 2A \sin\psi$, and, thus, $\delta = 0$ when $\theta_{\text{fp}} = 0$; also, $\theta_{\text{fp}} \le 2A$:

$$\boldsymbol{u} = \begin{Bmatrix} +\omega_0 \\ -i \\ ik_4 V_0/(V_0 + i\lambda\omega_0) \end{Bmatrix} \tag{107}$$

$$\boldsymbol{v} = \begin{Bmatrix} 1 \\ -k_3/(V_0 + i\lambda\omega_0) \\ iI_\theta\omega_0 \end{Bmatrix} \tag{108}$$

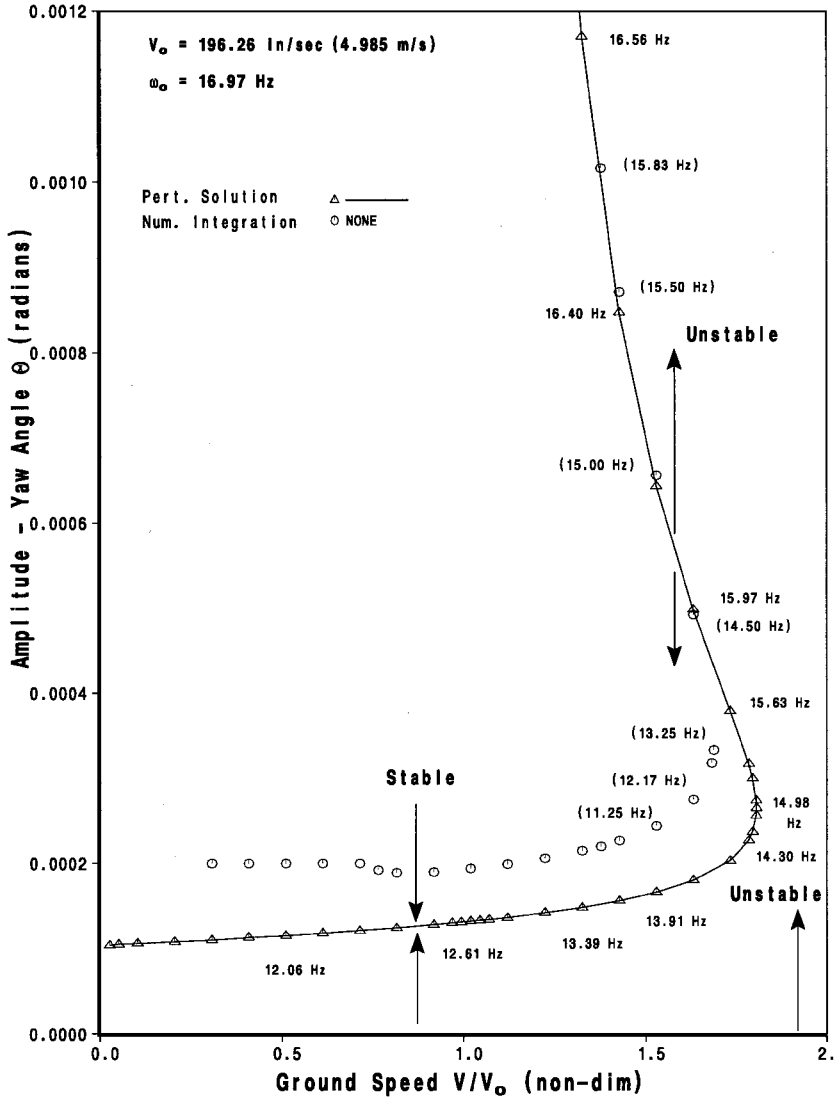

Fig. 3 Limit-cycle amplitude vs taxi speed: $C_{\text{cf}} = 100$ lb · in. and $\theta_{\text{fp}} = 0.0001$ rad.

Here, α, β, γ, and δ are computed using Eqs. (31–34) and (107) and (108). Note that $\boldsymbol{u}$ has been normalized so that $q_{20} = 2A \sin\psi$. Also, for this case with both coulomb friction and freeplay present, it has been assumed that $\text{sgn}(q_1) = 0$ when $|q_2| < \theta_{\text{fp}}$:

$$\alpha = \alpha_R + i\alpha_I \tag{109}$$

$$\alpha_I = -C_\theta - \frac{\lambda k_3 k_4 V_0 \left(V_0^2 - \lambda^2\omega_0^2\right)}{\left(V_0^2 + \lambda^2\omega_0^2\right)^2} \tag{110}$$

$$\alpha_R = 2I_\theta\omega_0 - \frac{2k_3k_4V_0^2\lambda^2\omega_0}{\left(V_0^2 + \lambda^2\omega_0^2\right)^2} \tag{111}$$

$$\beta = \frac{V_1 k_3 k_4 \left[\left(\lambda^3\omega_0^3 - \lambda\omega_0 V_0^2\right) + 2i\lambda^2 V_0\omega_0^2\right]}{\alpha\left(V_0^2 + \lambda^2\omega_0^2\right)^2} \tag{112}$$

$$\gamma = \gamma_R + i\gamma_I = \frac{2C_{\text{cf}}}{\pi\epsilon\alpha}\left[1 - \left(\frac{\theta_{\text{fp}}}{2A}\right)\right] \tag{113}$$

$$\gamma_R = \frac{2C_{\text{cf}}}{\pi\epsilon}\left[1 - \left(\frac{\theta_{\text{fp}}}{2A}\right)\right]\frac{\alpha_R}{\left(\alpha_R^2 + \alpha_I^2\right)} \tag{114}$$

$$\gamma_I = \frac{-2C_{\text{cf}}}{\pi\epsilon}\left[1 - \left(\frac{\theta_{\text{fp}}}{2A}\right)\right]\frac{\alpha_I}{\left(\alpha_R^2 + \alpha_I^2\right)} \tag{115}$$

$$\delta = \delta_R + i\delta_I \tag{116}$$

$$\delta_R = g_1 A\psi_{\text{fp}} + g_1\left(\frac{\theta_{\text{fp}}}{2}\right)\sqrt{1 - \left(\frac{\theta_{\text{fp}}}{2A}\right)^2} \tag{117}$$

$$\delta_I = g_2 A\psi_{\text{fp}} + g_2\left(\frac{\theta_{\text{fp}}}{2}\right)\sqrt{1 - \left(\frac{\theta_{\text{fp}}}{2A}\right)^2} \tag{118}$$

$$\psi_{\text{fp}} = \sin^{-1}\left(\frac{\theta_{\text{fp}}}{2A}\right) \tag{119}$$

$$g_1 = \frac{2k_\theta}{\pi\epsilon}\left(\frac{\alpha_I}{\alpha_R^2 + \alpha_I^2}\right) \tag{120}$$

$$g_2 = \frac{2k_\theta}{\pi\epsilon}\left(\frac{\alpha_R}{\alpha_R^2 + \alpha_I^2}\right) \tag{121}$$

$$\epsilon = \frac{V - V_0}{V_1} \tag{122}$$

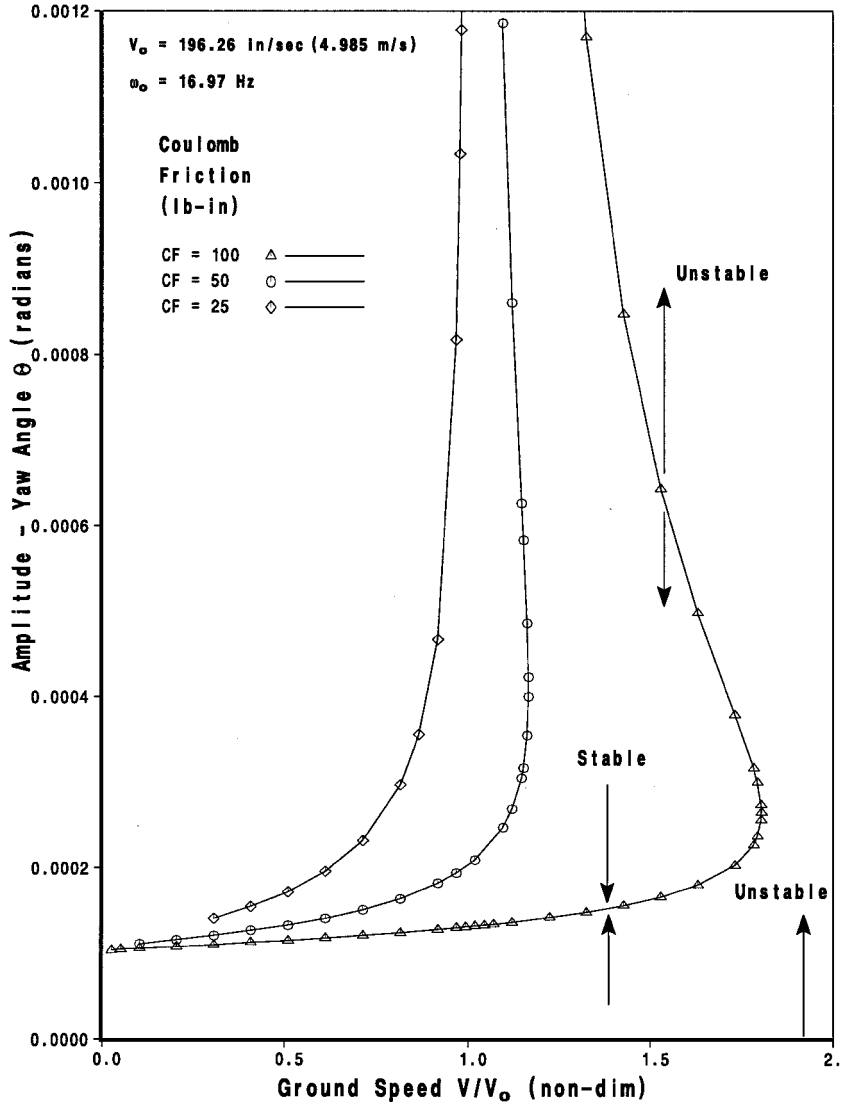

Fig. 4 Limit-cycle amplitude vs taxi speed: $\theta_{\text{fp}} = 0.0001$ rad and coulomb friction effects.

The limit-cycle amplitudes are given by the real positive roots of Eq. (39) and the frequency ω by Eq. (41), where $\psi = \omega\tau_0$.

A plot of limit-cycle amplitude θ vs taxi speed for $C_{cf} = 100\,\text{lb}\cdot\text{in.}$ (11.298 N · m) and $\theta_{fp} = 1.0 \times 10^{-4}$ rad is presented in Fig. 3. Also shown in Fig. 3 is a comparison of the perturbation solution with results from direct numerical integration of the nonlinear equations. Here, with both coulomb friction and freeplay present, the behavior of the system differs considerably from that either with coulomb friction only or with freeplay only. In particular, both stable and unstable limit cycles can exist for a given taxi speed and a finite amplitude limit cycle exists at the critical speed $V = V_0$.

At low taxi speeds, a stable limit cycle exists. As the ground speed V increases, the amplitude of the stable limit cycle increases gradually. For speed ratios $V/V_0 > 1$, both stable and unstable limit cycles exist. As the speed increases above V_0, the amplitude of the unstable limit cycle decreases and that of the stable limit cycle increases up to a speed ratio of about $V/V_0 = 1.8$, where a turning point is reached. The system is unstable for higher speed ratios beyond this point.

The amplitudes of the stable limit cycles determined by the perturbation solution are seen to differ somewhat from those obtained by the numerical integration solution at velocity ratios below the turning point at $V/V_0 < 1.8$. As the ground speed ratio decreases below about $V/V_0 = 0.8$, there is a change in the response characteristic to a relaxation-type oscillation and the frequency (not shown in Fig. 3) predicted by the perturbation solution does not agree nearly as well with that obtained by numerical integration: 13.91 Hz vs 12.17 Hz at $V/V_0 = 1.63$, 13.19 Hz vs 9.75 Hz at $V/V_0 = 1.32$, and 12.5 Hz vs 7.13 Hz at $V/V_0 = 0.92$. This behavior is in contrast to that observed for the case with freeplay present but no coulomb friction where the mode change did not occur until a very low speed ratio $V/V_0 < 0.2$.

The perturbation solution presented here assumes that the frequency does not deviate too greatly from the value ω_0 associated with the critical speed V_0.

For speed ratios in the range $V/V_0 = 0.9$–1.8, the amplitudes of the stable limit cycles predicted by the perturbation analysis are about 35% lower than those obtained from the numerical integration solution (33% at $V/V_0 = 0.92$, 32% at $V/V_0 = 1.02$, 31% at $V/V_0 = 1.32$, and 35% at $V/V_0 = 1.63$) until the turning point is reached, after which agreement between the unstable limit-cycle amplitudes is very good.

For the case here, with both coulomb friction and freeplay present, the turning point predicted by the perturbation solution occurs at $V/V_0 = 1.81$ compared with $V/V_0 = 1.69$ from the numerical integration solution, about 7% higher.

Figure 4 is a plot of coulomb friction variation effects on limit-cycle amplitude θ vs taxi speed for $C_{cf} = 25$, 50, and 100 $\text{lb}\cdot\text{in.}$ (2.8245, 5.649, and 11.298 N · m) and $\theta_{fp} = 1.0 \times 10^{-4}$ rad. For the lowest value of coulomb friction, $C_{cf} = 25\,\text{lb}\cdot\text{in.}$, only a stable limit cycle exists for speed ratios $V/V_0 < 1$, and the system is unstable for speed ratios $V/V_0 > 1$. For higher levels of coulomb friction, that is,

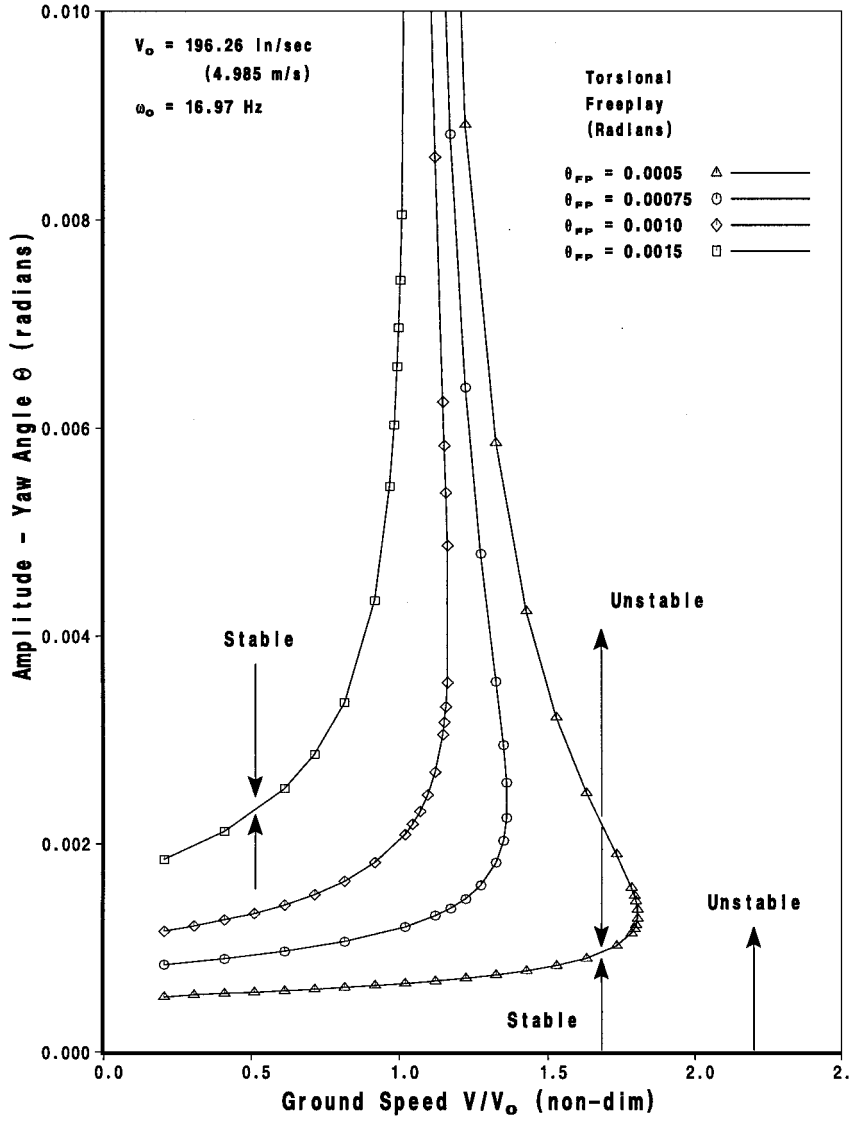

Fig. 5 Limit-cycle amplitude vs taxi speed: $C_{cf} = 500\,\text{lb}\cdot\text{in.}$ and freeplay variation effects.

$C_{cf} = 50$ lb · in. or more, both stable and unstable limit cycles occur. With increasing coulomb friction levels, the amplitude of the stable limit cycle decreases, and the turning point occurs at a higher speed ratio.

Figure 5 is a plot of torsional freeplay variation effects on limit-cycle amplitude θ vs taxi speed for $C_{cf} = 500$ lb · in. (56.49 N · m) and for $\theta_{fp} = 0.0005$, 0.00075, 0.0010, and 0.0015 rad. For the highest freeplay value, that is, $\theta_{fp} = 0.0015$ rad, only a stable limit cycle exists for speed ratios $V/V_0 < 1$, and the system is unstable for speed ratios $V/V_0 > 1$. For lower levels of freeplay, that is, $\theta_{fp} = 0.0010$ rad or less, both stable and unstable limit cycles occur. With decreasing freeplay levels, the amplitude of the stable limit cycle decreases, and the turning point occurs at a higher speed ratio.

VI. Summary

A perturbation analysis of nonlinear wheel shimmy in aircraft landing gear was presented for nonlinear models that include terms due to coulomb friction between the oleo struts and freeplay in the torque links. The method of multiple-timescales was used to obtain general expressions for the limit-cycle amplitude and the frequency that are functions of ground speed. The analysis showed that stable or unstable limit cycles can exist for taxi speeds above or below a critical value with stability of the limit cycles being determined by the sign of a computed coefficient. It was shown that, when only coulomb friction is present, an unstable limit cycle exists and that, when only freeplay is present, a stable limit cycle exists. When both coulomb friction and freeplay are present, it was shown that stable and unstable limit cycles and a turning point can exist depending on the system parameter values. The solution method was applied to a simple shimmy model and results from the perturbation analysis were shown to be in good agreement with those obtained by direct numerical integration of the nonlinear shimmy equations.

Appendix A: Nonlinear Shimmy Model Equations of Motion

A simple shimmy model with nonlinear terms due to coulomb friction and torsional freeplay is presented. The model shown in Fig. A1 is a modification of one studied by Nybakken[20] and consists of a wheel attached to a pivoted rigid arm. The system has a moment of inertia I_θ about the pivot, mechanical trail L_m, pneumatic trail L_p, torsional stiffness K_θ about the pivot, and a linear viscous damper C_θ in parallel with the pivot stiffness K_θ. Modifications to the model include nonlinear terms for the torsional moment due to coulomb friction in the strut oleos and a torsional moment including the effect of freeplay in the torque links. A finite contact patch is assumed and the tangent approximation to Von Schlippe's linear string theory (see Nybakken[20]) is used for the tire model. Default values for the various model parameters are given in Appendix B.

A string-type theory has two basic relations that govern tire behavior. One states that the tire force output is proportional to a characteristic deflection of the contact patch relative to the wheel plane. The proportionality constant is the static lateral stiffness k_y of the tire. Because the center of the contact patch of a static tire under lateral deformation is a straight line, the assumption is made that the contact patch centerline is a straight line under rolling conditions. Assuming a straight contact line, the tire force F is given by

$$F = k_y(z + \bar{z})/2 \tag{A1}$$

where z is the centerline deflection at the front of the contact line, $\bar{z}$ is the deflection at the rear of the contact line, and k_y is the static lateral stiffness of the tire.

The other basic relation governing tire behavior is the prediction that the centerline deflection outside the contact patch decays in an exponential curve. This can be expressed as

$$-\frac{dz}{ds} = \frac{z}{\lambda} \tag{A2}$$

where λ is called the relaxation length. It defines a given tire and is analogous to a time constant. When Fig. A1 is referred to, the deflection $\bar{z}$ at the rear of the contact patch is determined by extrapolating from the front using the slope at the front (the tangent approximation):

$$\bar{z} = z - 2h\frac{dz}{ds} \tag{A3}$$

When Eq. (A2) is used for the slope, Eq. (A3) becomes

$$\bar{z} = z(1 + 2h/\lambda) \tag{A4}$$

For small angles,

$$\frac{dy}{ds} = \alpha - \theta \tag{A5}$$

or

$$\frac{z}{\lambda} = -\frac{dz}{ds} = \frac{dy}{ds} + \theta \tag{A6}$$

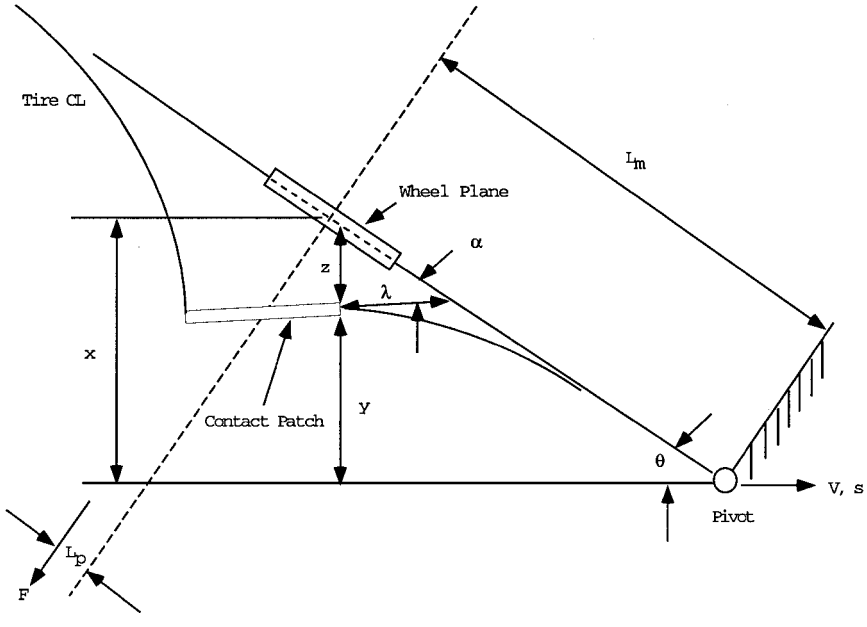

Fig. A1 Third-order shimmy model (Nybakken[20]).

and

$$z = x - y - h\theta \tag{A7}$$

Substituting Eqs. (A5–A7) into Eqs. (A1) and (A2) and transforming to the time domain with $s = Vt$, assuming V to be a constant, gives the tire force F and the kinematic equation relating y, x, and θ. The tire force F is given by

$$F = k_y(x - y - h\theta)(1 + h/\lambda) \tag{A8}$$

and the kinematic relation is given by

$$\dot{y} + Vy/\lambda = Vx/\lambda - V\theta(1 + h/\lambda) \tag{A9}$$

The equation of motion for this simple model is

$$I_\theta\ddot{\theta} + C_\theta\dot{\theta} + F_{\text{cf}} + F_{\text{fp}} = -F\bar{L} \tag{A10}$$

where F_{cf} is the moment due to coulomb friction, F_{fp} is the structural moment about the pivot, including freeplay effects, and $\bar{L}$ is the effective trail:

$$\bar{L} = L_m + L_p \tag{A11}$$

$$\begin{aligned} F_{\text{fp}} &= k_\theta(\theta - \theta_{\text{fp}}), && \theta > +\theta_{\text{fp}} \\ &0, && |\theta| \le +\theta_{\text{fp}} \\ &k_\theta(\theta + \theta_{\text{fp}}), && \theta < -\theta_{\text{fp}} \end{aligned} \tag{A12}$$

In state variable notation, the nonlinear shimmy equations under consideration here have the form

$$\bar{\boldsymbol{M}}\dot{\boldsymbol{q}} + \bar{\boldsymbol{K}}\boldsymbol{q} = \boldsymbol{f}_{\text{cf}} + \boldsymbol{f}_{\text{fp}} \tag{A13}$$

where $\boldsymbol{q}$ is a vector of the time-dependent state variables and $\bar{\boldsymbol{M}}$ is a matrix containing inertia and viscous damping terms. The matrix $\bar{\boldsymbol{K}}$ contains structural and tire stiffness terms including taxi-velocity-dependent terms, $\boldsymbol{f}_{\text{cf}}$ is a vector of nonlinear coulomb friction terms, and $\boldsymbol{f}_{\text{fp}}$ is a vector of nonlinear stiffness terms, which include torsional freeplay effects in the landing gear torque links, which connect the outer and inner oleo struts.

The degrees of freedom defined by the state vector $\boldsymbol{q}$ are θ, $\dot{\theta}$, and y, which are torsional rotation of the wheel, torsional velocity, and lateral deflection of the tire at the center of the tire–ground contact patch, respectively,

$$\boldsymbol{q} = \{\dot{\theta} \quad \theta \quad y\}^T \tag{A14}$$

$$\boldsymbol{f}_{\text{cf}} = -\{F_{\text{cf}} \quad 0 \quad 0\}^T \tag{A15}$$

$$F_{\text{cf}} = C_{\text{cf}}\,\text{sgn}(\dot{\theta}) \tag{A16}$$

$$\begin{aligned} \text{sgn}(\dot{\theta}) &= +1, && \dot{\theta} > 0 \\ &0, && \dot{\theta} = 0 \\ &-1, && \dot{\theta} < 0 \end{aligned} \tag{A17}$$

$$\boldsymbol{f}_{\text{fp}} = -\{F_{\text{fp}} \quad 0 \quad 0\}^T \tag{A18}$$

where F_{fp} is given by Eq. (A12), and

$$\bar{\boldsymbol{M}} = \begin{bmatrix} I_\theta & C_\theta & 0 \\ 0 & 0 & \lambda \\ 0 & 1 & 0 \end{bmatrix} \tag{A19}$$

$$\bar{\boldsymbol{K}} = \begin{bmatrix} 0 & k_2 & k_3 \\ 0 & k_4 V & V \\ -1 & 0 & 0 \end{bmatrix} \tag{A20}$$

Rewrite F_{fp} as

$$F_{\text{fp}} = k_\theta\theta + \hat{F}_{\text{fp}} \tag{A21}$$

where

$$\begin{aligned} \hat{F}_{\text{fp}} &= -k_\theta\theta_{\text{fp}}, && \theta > +\theta_{\text{fp}} \\ &-k_\theta\theta, && |\theta| \le +\theta_{\text{fp}} \\ &+k_\theta\theta_{\text{fp}}, && \theta < -\theta_{\text{fp}} \end{aligned} \tag{A22}$$

Then, with

$$k_2 = k_y\bar{L}(1 + h/\lambda)(L_m - h) \tag{A23}$$

$$k_3 = -k_y\bar{L}(1 + h/\lambda) \tag{A24}$$

$$k_4 = -L_m + \lambda + h \tag{A25}$$

$$k_1 = k_2 + k_\theta \tag{A26}$$

$$\hat{\boldsymbol{F}}_{\text{fp}} = -\{\hat{F}_{\text{fp}} \quad 0 \quad 0\}^T \tag{A27}$$

$$\hat{\boldsymbol{F}}_{\text{cf}} = -\{C_{\text{cf}} \quad 0 \quad 0\}^T \tag{A28}$$

$$\boldsymbol{K} = \begin{bmatrix} 0 & k_1 & k_3 \\ 0 & k_4 V & V \\ -1 & 0 & 0 \end{bmatrix} \tag{A29}$$

and with $\boldsymbol{M} = \bar{\boldsymbol{M}}$, substitution of Eqs. (A14–A29) into Eq. (A13) gives

$$\boldsymbol{M}\dot{\boldsymbol{q}} + \boldsymbol{K}\boldsymbol{q} = \hat{\boldsymbol{F}}_{\text{cf}}\,\text{sgn}(\dot{\theta}) + \hat{\boldsymbol{F}}_{\text{fp}} \tag{A30}$$

or

$$\boldsymbol{M}\dot{\boldsymbol{q}} + \boldsymbol{K}\boldsymbol{q} = \hat{\boldsymbol{F}}_j\,\text{sgn}(q_j) + \hat{\boldsymbol{F}}_k(\hat{F}_{\text{fp}}, q_k) \tag{A31}$$

where

$$\begin{aligned} \text{sgn}(q_j) &= +1, && q_j > 0 \\ &0, && q_j = 0 \\ &-1, && q_j < 0 \end{aligned} \tag{A32}$$

and $\hat{\boldsymbol{F}}_j = \hat{\boldsymbol{F}}_{\text{cf}}$ and $\hat{\boldsymbol{F}}_k(\hat{\boldsymbol{F}}_{\text{fp}}, q_k) = \hat{\boldsymbol{F}}_{\text{fp}}$. Note that $j = 1$ and $k = 2$, referring to $q_1 = \dot{\theta}$ and $q_2 = \theta$, respectively, for the simple model being considered here. Also, $\boldsymbol{K}$ now includes the linear stiffness k_θ in the term k_1 defined in Eq. (A26).

Appendix B. Shimmy Model Parameters

Table B1 Dependent variables

Quantity	Description and Units
θ	Wheel torsional rotation, rad
$\dot{\theta}$	Torsional velocity, rad/s
y	Lateral deflection at front of tire contact patch, in.(m)

Table B2 Landing gear parameters

Parameter	Description and Units
C_θ	Torsional damping coefficient, 2268 lb · in./rad/s (256.25 N · m/rad/s)
C_{cf}	Strut coulomb friction coefficient, 100.0 lb · in. (11.298 N · m)
F_{fp}	Effective moment in torque link, lb · in. (N · m)
F_{cf}	Moment due to coulomb friction between oleos, lb · in. (N · m)
h	Half-length of the tire contact patch, 6.72 in. (0.170688 m)
I_θ	Moment of inertia of gear 189 lb · in. · s^2 (21.354 N · m · s^2)
k_θ	Torsional stiffness of gear 2.4741×10^6 lb · in./rad (2.7954×10^5 N · m/rad)
k_y	Lateral stiffness of tire 6861.4 lb/in. (1.2016×10^6 N/m)
L_m	Mechanical trail of wheel 3.0 in. (0.0762 m)
L_p	Pneumatic trail of tire 5.75 in. (0.14605 m)
λ	Relaxation length of tire 10.24 in. (0.260096 m)
θ_{fp}	Effective torsional freeplay, rad

References

[1]Pacejka, H. B., "The Wheel Shimmy Phenomenon," Ph.D. Dissertation, Delft Technical Inst., Delft, The Netherlands, Dec. 1966.

[2]Krylov, N. M., and Bogoliubov, N. N., *Introduction to Nonlinear Mechanics*, Academy of Science, Ukraine, U.S.S.R., 1937 (translated by S. Lefschetz, Princeton Univ. Press, Princeton, NJ, 1947).

[3]Collins, R. L., "Theories on the Mechanics of Tires and Their Applications to Shimmy Analysis," *Journal of Aircraft*, Vol. 8, No. 4, 1971, pp. 271–277.

[4]Gordon, J. T., and Merchant, H. C., "An Asymptotic Method for Predicting Amplitudes of Nonlinear Wheel Shimmy," *Journal of Aircraft*, Vol. 15, No. 3, 1978, pp. 155–159.

[5]Burton, T. D., "Describing Function Analysis of Nonlinear Nose Gear Shimmy," American Society of Mechanical Engineers, ASME Paper 81-WA/DSC-20, 1981.

[6]Somieski, G., "Shimmy Analysis of a Simple Aircraft Nose Landing Gear Model Using Different Mathematical Methods," *Aerospace Science and Technology*, Vol. 8, 1997, pp. 545–555.

[7]Popov, E. P., "On the Use of the Harmonic Linearization Method in Automatic Control Theory," NACA TM 1406, Jan. 1957.

[8]Shen, S. F., "An Approximate Analysis of Nonlinear Flutter Problems," *Journal of the Aerospace Sciences*, Vol. 25, 1959, pp. 25–32, 45.

[9]Šiljak, D. D., *Nonlinear Systems*, Wiley, New York, 1969, pp. 107–151.

[10]Bogoliubov, N. N., and Mitropolsky, Y. A., *Asymptotic Methods in the Theory of Nonlinear Oscillations*, Hindustan, New Delhi, India, 1961.

[11]Morrison, J. A., "Comparison of the Modified Method of Averaging and the Two Variable Expansion Procedure," *SIAM Review*, Vol. 8, 1966, pp. 66–85.

[12]Cole, J. D., and Kevorkian, J., "Uniformly Valid Asymptotic Approximations for Certain Nonlinear Differential Equations," *Proceedings of the International Symposium—Nonlinear Differential Equations and Nonlinear Mechanics*, Academic Press, 1963, New York, pp. 113–120.

[13]Kevorkian, J., "The Two Variable Expansion Procedure for the Approximate Solution of Certain Nonlinear Differential Equations," *Space Mathematics, Pt. 3, Lectures in Applied Mathematics*, American Mathematical Society, Providence, RI, 1966.

[14]Nayfeh, A. H., "A Perturbation Method for Treating Nonlinear Oscillation Problems," *Journal of Mathematical Physics*, Vol. 44, 1965, pp. 368–374.

[15]Nayfeh, A. H., *Perturbation Methods*, 1st ed. Wiley, New York, 1973.

[16]Nayfeh, A. H., and Mook, D. T., *Nonlinear Oscillations*, 1st ed. Wiley, New York, 1979.

[17]Morino, L., "Perturbation Method for Treating Nonlinear Panel Flutter Problems," *AIAA Journal*, Vol. 7, No. 3, 1969, pp. 405–411.

[18]Kuo, C. C., Morino, L., and Dugundji, J., "Perturbation and Harmonic Balance Methods for Nonlinear Panel Flutter," *AIAA Journal*, Vol. 10, No. 11, 1972, pp. 1479–1484.

[19]Smith, L. L., and Morino, L., "Stability Analysis of Nonlinear Differential Autonomous Systems with Application to Flutter," *AIAA Journal*, Vol. 14, No. 3, 1976, pp. 333–341.

[20]Nybakken, G. H., "Investigation of Tire Parameter Variations in Wheel Shimmy," Ph.D. Dissertation, Dept. of Applied Mechanics, Univ. of Michigan, Ann Arbor, MI, 1973.

[21]"Easy5X User Guide," Boeing Computer Services Document BCS 20491-0530-R1, The Boeing Co., Seattle, WA, Jan. 1993.

[22]"BCSLIB Mathematical/Statistical Library Users Guide," Boeing Computer Services Document BCS 20462-0516-R14, Vol. 1, The Boeing Co., Seattle, WA, June 1993.